JPET #118109

Bradycardic Therapy Improves Left Ventricular Function and Remodeling in Dogs with Coronary Embolization-Induced Chronic Heart Failure

Isaac George*, Yanping Cheng*, Geng-Hua Yi, Steven Reiken, Anguo Gu, Yuankai Kenny Tao, Jordan Muraskin, Siyi Qin, Kun-Lun He, Ilan Hay, Kenward Yu, Mehmet C. Oz, Daniel Burkhoff, Jeffrey Holmes, and Jie Wang

The Institute of Molecular and Experimental Therapeutics, East China Normal University, Shanghai, P.R. of China (J.W.); The Jack Skirball Center for Cardiovascular Research, Orangeburg, NY (J.W.); Department of Medicine, Division of Cardiology, Columbia University College of Physicians and Surgeons, New York, NY (Y.C., GH.Y., S.R., A.G., Y.K.T., S.Q., KL.H., I.H., K.Y., D.B., J.W.); Department of Surgery, Division of Cardiothoracic Surgery, Columbia University College of Physicians and Surgeons, New York, NY (I.G., J.M., M.C.O.); and Department of Biomedical Engineering, Columbia University, New York, NY (J.H.)

1

Running Title: Bradycardic Therapy and CHF

Correspondence Address:

Jie Wang, MD, PhD

The Jack H. Skirball Center for Cardiovascular Research

Cardiovascular Research Foundation

8 Corporate Drive

Orangeburg, NY 10962

Tel: (845)-290-8100

Fax: (845)-290-8030

Email: jwang@crf.org

Text Pages (count): 15

Tables (count): 3

Figures (count): 4

References (count): 28

Abstract (word count): 236

Introduction (word count): 294

Discussion (word count): 1570

Non-standard Abbreviations:

α	chamber stiffness
β	EDPVR scaling constant
Cilo	Cilobradine

EDPVR	end-diastolic pressure-volume relationship
EDV	end-diastolic volume
E_{es}	end-systolic elastance
EF	ejection fraction
ESPVR	end-systolic pressure-volume relationship
ESV	end-systolic volume
IVC	inferior vena cava
LAD	left Anterior Descending Coronary Artery
LVEDD	left ventricular end-diastolic diameter
LVEDP	left ventricular end-diastolic pressure
LVSP	left ventricular systolic pressure
MAP	mean arterial pressure
Meto	Metoprolol
NCX1	Na^+-Ca^{2+} exchanger
PAGE	SDS-polyacrylamide gel electrophoresis
P_{ed}	pressure at end-diastole
PKA	RyR2 protein kinase A
PV	pressure-volume
RyR2	ryanodine receptor
SERCA2a	cardiac sarcoplasmic reticulum calcium-ATPase
τ	isovolemic relaxation constant
TBS-T	Tris-buffered saline with 0.1% Tween-20
V_{ed}	volume at end-diastole

V_0 ESPVR volume intercept

Section Assignment: Cardiovascular

Abstract

Both β-adrenergic blockade and bradycardia may contribute to the therapeutic effect of β-blockers in chronic heart failure (CHF). This study tested the relative importance of bradycardia by comparing cilobradine (Cilo), a sinus node inhibitor, to a β-blocker, metoprolol (Meto), in an established canine model of CHF. Dogs were chronically instrumented for hemodynamic and LV volume measurements. CHF was created by daily coronary embolization via a chronically implanted coronary (LAD) catheter. After establishment of CHF, control (n=6), Meto (30mg/day, n=5), Cilo (Low) (1 mg/kg/day, n=5), or Cilo (High) (3 mg/kg/day, n=5) was given orally for 12 weeks. Systemic hemodynamics, echocardiography and pressure volume analysis were measured at baseline, at CHF, and three months after treatment in an awake state. Protein levels of cardiac sarcoplasmic reticulum calcium-ATPase (SERCA2a), ryanodine receptor (RyR2) and Na^+-Ca^{2+} exchanger (NCX1) were measured by western blot. RyR2 protein kinase A (PKA) phosphorylation was determined by back-phosphorylation. After 12 weeks, Meto and Cilo (High and Low) produced similar bradycardic effects, accompanied by a significantly improved LV dP/dt versus Control (Meto: 2602±70, Cilo (Low): 2517±45, Cilo (High): 2579±78, Control: 1922±115 mmHg/s, $p<0.05$). Both Meto and Cilo (High) normalized protein levels of SERCA2a, NCX1 and reversed PKA hyperphosphorylation of RyR2, in contrast to controls. High-dose Cilobradine effectively produced bradycardia and improved cardiac function after CHF, comparable to metoprolol. Restored protein levels of SERCA2a and improved function of RyR2 may be an important mechanism associated with cilobradine therapy.

Introduction

β-adrenergic blocker therapy reduces morbidity and mortality in patients with chronic heart failure (CHF) (Packer et al., 1996). A number of molecular mechanisms have been proposed to account for these benefits, including restoration of β-receptor density and signal transduction (Heilbrunn et al., 1989), normalization of abnormal phosphorylation status (Reiken et al., 2001), improved calcium channel function (Reiken et al., 2003), and correction of neurohormonal imbalance (Bristow, 1984). The role of β-blocker-induced bradycardia in improving left ventricular (LV) dysfunction in CHF has also been investigated. Nagatsu et al. (Nagatsu et al., 2001) reported that if β-blocker-induced bradycardia was prevented by cardiac pacing in a canine model of CHF, no improvement in LV function was seen, highlighting the importance of heart rate reduction in CHF therapy. Prevention of tachycardia may contribute to clinical benefit after β-blockade, as tachycardia can be both a cause and secondary effect of progressive CHF (Packer et al., 1986). These studies suggest a role for bradycardic therapy in the treatment of CHF (Lechat, 2003).

β-blocker therapy, however, poses special challenges in the heart failure population, mainly due to its effects on systolic function. Certain populations of patients, such as those with reactive airway disease, conduction system disease, or hemodynamic compromise, may not tolerate therapy. This has lead to the need for dose titration and limitations on its clinical use. An ideal agent for these patients can produce the same physiologic effects as a β-blocker without the negative effects of β-receptor blockade. Accordingly, the purpose of this study was to test whether cilobradine, a sinus node inhibitor, produces beneficial effects on cardiac function in a canine model of embolization-induced heart failure similar to β-adrenergic blocker therapy. Levels of calcium-handling proteins and phosphorylation status of the ryanodine receptor

6

(RyR2), shown to normalize with β-blockade (Reiken, 2001 and 2003), were also examined as

potential mechanisms of benefit.

Methods

Study Design

Multiple daily coronary-embolizations were used in 21 mongrel dogs of both sexes (22-27 kg) to create CHF. After a stable CHF state was maintained for 7 days, each animal was assigned to one of four groups: 1) Control, who received normal saline (n=6), 2) metoprolol (Meto, n=5, 30 mg/day PO) (Novartis Pharmaceuticals, East Hanover, NJ), 3) low dose cilobradine (Cilo-Low) (Boehringer Ingelheim, Ingelheim, Germany), (n=5, 1 mg/kg/day PO), and 4) high dose cilobradine (Cilo-High) (n=5, 3 mg/kg/day PO). Hemodynamic measurements and echocardiograms were performed prior to CHF, after an established stable CHF, and 12 weeks after treatment with cilobradine, metoprolol, or saline. At the end of 12 weeks, the animals were sacrificed, and LV myocardial tissue from the non-embolized region was harvested for assessment of calcium-handling protein levels and phosphorylation of RyR2. This study was approved by the institutional Animal Care and Use Committee of Columbia University, and conforms with the "Guide for Care and Use of Laboratory Animals" published by the National Institutes of Health (NIH publication 85-23, revised 1996).

Surgical Preparation

On the day of surgery, each animal (22-25 kg) was premedicated with Telazol 3-5 mg/kg IM (tiletamine hydrochloride and zolazepam hydrochloride, Wyeth, Madison, NJ), induced with sodium thiopental 15-20 mg/kg IV (Abbott Laboratories, Abbott Park, IL), and ventilated on isoflurane at 1.5-2.5% (Abbott Laboratories, Abbott Park, IL). The instrumentation surgery began with a left thoracotomy between the 4th and 5th intercostal space to expose the heart. A Konigsberg solid state pressure gauge (6.5, Konigsberg Instruments Inc., Pasadena, CA) was placed through the LV apex for measurement of LV pressure. Fluid-filled catheters were placed

in the ascending aorta and the LV for measurement of aortic pressure and calibration of the Konigsberg pressure gauge, respectively. A pneumatic cuff was placed around the inferior vena cava (IVC) to vary loading conditions postoperatively. The left anterior descending coronary artery (LAD) was isolated, and a thin silastic cannula was inserted through an arteriotomy for microsphere embolization administration. In addition, 6 sonomicrometric crystals (Sonometrics Corp., London, Canada) were placed on the anterior, posterior, apex, base, septal and free walls of the LV. These surgical procedures and cardiac instrumentations have been used in our laboratory previously (He et al., 2005).

Coronary Embolization-Induced Heart Failure

This model has been described previously in detail (Knecht et al., 1997). In brief, CHF was produced by daily intracoronary microembolization with 25,000-50,000 (90-120 μm in diameter) polymer bead injections through the previously implanted LAD cannula. Embolization proceeded until LV end-diastolic pressure (LVEDP) reached 15 mmHg and LV dP/dt was less than 2400 mmHg/s. Embolization was halted at this time, and hemodynamics and echocardiography were repeated in an awake state after an additional 7 days to confirm the stability of the CHF state.

Hemodynamics and Echocardiography

Hemodynamics and echocardiography were measured as previously described in an awake state (He et al., 2005). In brief, on the day of each experiment, the dog was brought to the laboratory and placed on the table. All measurements were taken after the dogs were quiet for an average of 60 minutes and accustomed to the laboratory. Arterial pressure was measured by attaching the previously implanted catheters to P23ID strain-gauge transducers (Statham Instruments, Inc., Oxnard, CA). LV systolic pressure (LVSP) was measured with the previously

implanted solid-state pressure gauges, which were calibrated *in-vitro* against an electronic signal

of known size and cross-calibrated *in-vivo* with measurements of pressure from the LV catheter.

Inflating the previously placed pneumatic cuff transiently occluded the IVC for construction of

LV pressure-volume (PV) relationships. Mean arterial pressure (MAP) was determined on-line

by use of 3-Hz averaging filters (DA26, Medtron Engineering, Olivenhain, CA). Continuous

electrocardiographic data was obtained using leads placed on the skin. Data was recorded on an

eight-channel thermal writing chart recorder (30-V8808-10, Gould Electronics, East Rutherford,

NJ), and periods of interest were digitized (Gateway 2000 486 computer equipped with an

analog-to-digital conversion system, Sonometric Corp., London, Ontario, Canada) for off-line

analysis. Heart rate was determined manually from the electrocardiographic tracing over a 60

second period and averaged over 3 readings during a two hour period. Echocardiograms were

performed using a Hewlett Packard Sonos 5500 at baseline, CHF state, and every 4 weeks after

CHF in an awake state. Echocardiograms were analyzed off-line by a blinded observer by

quantifying short axis end-diastolic and end-systolic area at mid-papillary levels with a 3.5-MHz

transducer. Ejection fraction (EF) was similarly calculated as end-diastolic volume (EDV)

minus end-systolic volume (ESV), divided by EDV ([EDV-ESV]/EDV*100).

Pressure-Volume Loop Analysis

LV pressure and LV volume were measured at baseline, CHF state, and every 4 weeks

after device implantation via previously implanted solid state pressure gauges in the LV and

sonomicrometric crystals in an awake state, as previously described (He et al., 2005). Briefly,

LV PV relationship loops were measured at rest and during a transient preload reduction induced

by IVC occlusion. LV volumes (LV_{vol}) were estimated from sonomicrometrically measured

dimensions assuming an ellipsoid model: $LV_{vol}= \pi AP \cdot SF \cdot AB/6,$ where AP is anterior–posterior,

SF is septal-free wall, and AB is apex-base dimensions. The end-systolic pressure-volume relationship (ESPVR) was assessed using a linear approach: $E_{es} = P_{es}/(V_{es}-V_0)$, where the slope (end-systolic elastance, E_{es}) defines contractility, and V_0 its volume-axis intercept. The end-diastolic pressure-volume relationship (EDPVR) was determined by applying non-linear regression analysis to the end-diastolic pressure and volume points (P_{ed} and V_{ed}, respectively) during a rapid IVC occlusion via pneumatic cuff inflation. These data were fit to the following equation: $P_{ed} = \beta e^{\alpha V_{ed}}$, where α is a chamber stiffness constant, and β is a scaling constant. Each steady state measurement was calculated and averaged over 10 cardiac cycles using custom software (Matlab, v.6.5).

Protein Isolation and Western Analysis for Calcium-Handling Proteins

Three calcium-handling protein levels of myocardium were examined: SERCA2a, NCX1, and RyR2. In brief, lysates of LV tissue samples from non-embolization zone were made by sonication of approximately 150 mg of each sample in a seven-fold volume of lysis buffer (20 mmol/L Na-HEPES, 4 mmol/L EGTA, 1 mmol/L DTT, pH 7.4) in the presence of proteinase inhibitors (0.1 mmol/L leupeptin and 0.3 mmol/L PMSF) for 1 minute on ice. The protein concentration was determined using bovine serum albumin as a standard. Samples (50 µg) denatured at 95°C were size-fractionated using SDS-polyacrylamide gel electrophoresis (PAGE) under reducing conditions. In order to determine the levels of SERCA2a, NCX1 and tubulin, SDS-PAGE was performed using 7.5% separating and 5% stacking gels; for RyR2, 5% separating and 4% stacking gels were used. Electrophoresis was performed in a Miniprotean II cell (Bio-Rad Ltd., Hercules, CA) followed by transfer of proteins (4°C for 2 hr at 100 V) onto nitrocellulose in a mini trans-blot transfer cell (Bio-Rad Ltd.) filled with transfer buffer (25 mmol/L Tris-HCl, pH 8.3, 150 mmol/L glycine and 20% methanol).

Blots were blocked overnight at 4°C in 5% nonfat milk diluted in Tris-buffered saline

(20 mmol/L Tris-HCl, pH 7.6 and 150 mmol/L NaCl) with 0.1% Tween-20 (TBS-T). Blots were

then incubated with primary antibody diluted in TBS-T (anti-SERCA2a, 1:8000-Mouse

monoclonal antibody (Novocastra Laboratories Ltd, Benton Lane, UK); anti-NCX1, 1:5000-

Rabbit antiserum (Swant Co., Bellinzona, Switzerland); anti-RyR2, 1:4000-Mouse monoclonal

antibody (Upstate Biotechnology, NY, USA); and anti-tubulin, 1:6000-Mouse monoclonal

antibody, Sigma, USA)) for 2 hours at room temperature. After washing in TBS-T, blots were

incubated in the presence of a peroxidase-labeled secondary antibody (Ammersham Pharmacia

Biotech, Piscatawy, NJ) diluted 1:10000 for 1 hr at room temperature. Blots were washed again

and incubated with ECL reagent (Amersham) for 1 min, followed by autoradiography.

Optical densities of protein signals on x-ray films were determined by a laser scanning

densitometer (Molecular Dynamics, Vernon Hills, IL) for quantification of protein levels. All

three protein levels were expressed relative to tubulin.

The phosphorylation status of RyR2 was also examined. Myocardial homogenates were

prepared, RyR2 was immunoprecipitated, and protein kinase A (PKA) phosphorylation was

determined as described previously (Reiken et al., 2003). In brief, 1 gram of LV tissue was

homogenized in 1.0 ml of a buffer containing 50 mM Tris-HCl (pH 7.4), 200 mM NaCl, 20 mM

NaF, 1.0 mM Na_3VO_4, 1.0 mM DTT and protease inhibitors. Samples were centrifuged (3,000 *g*

for 10 min and the supernatant was centrifuged (8,000 g for 10 min). RyR2 was

immunoprecipitated from samples by incubating 500 µg of homogenate with anti-RyR antibody

(2 µl 5029 Ab) in 0.5 ml of as modified RIPA buffer (50 mM Tris-HCl (pH 7.4), 0.9% NaCl, 5.0

mM NaF, 1.0 mM Na_3VO_4, 0.5% Triton-X100, and protease inhibitors) overnight at 4°C. The

samples were incubated with Protein A sepharose beads (Ammersham Pharmacia Biotech,

Piscatawy, NJ) at 4°C for 1 hour, after which, the beads were washed three times with RIPA.

Samples were heated to 95°C and size fractionated by PAGE. Immunoblots were developed

using either an anti-RyR (5029, 1:5000 dilution) or a phospho-specific Ab that recognizes PKA

phosphorylated RyR2 (P2809, 1:5000) (Reiken et al., 2003). Band densities were quantified by

densitometry.

Statistics

Values are reported as mean ± standard error. A one-way ANOVA with post-hoc

Bonferroni analysis was used for all comparisons of continuous variables between groups. A

paired Student's t test was used only to compare measurements obtained at baseline, CHF state,

and after 12 weeks within one cohort. A $p <0.05$ was considered statistically significant.

Analysis was performed using SPSS v. 11.5 (Chicago, IL).

Results

Hemodynamics

The hemodynamics at baseline, at CHF, and after 12 weeks of treatment are summarized

in Table 1. Representative steady-state PV loops are shown in Figure 1. After 6.0 ± 1.5 weeks

of coronary micro-embolization, PV loops in all groups shifted rightward. Treatment with Meto,

Cilo (Low), and Cilo (High) shifted PV loops back towards baseline, in contrast to PV loops

from Control animals, which shifted rightwards slightly over 12 weeks. Cilo (High and Low)

and Meto effectively decreased heart rate, compared to Control animals (Figure 2A). LV dP/dt

was uniformly improved after 12 weeks of treatment in Meto and Cilo (both Low and High)

groups after significant reductions with coronary embolization (Figure 2B). A significant

increase in MAP was seen after 12 weeks in Cilo (High) compared to Control ($p<0.05$) (Table 1).

Echocardiography

Echocardiographic measurements are presented in Table 2. All animals experienced an

equal and significant reduction in ejection fraction (EF) after embolization. EF recovered

significantly in Meto animals versus control group, and trends towards improvements were seen

in Cilo (Low and High), as seen in Figure 2C. It is important to note that LV end-diastolic

diameter remained constant in Metoprolol and Cilo (High-dose) animals, versus a significant

increase in Control animals and a trend towards increase in Cilo (Low-dose) animals.

Pressure-Volume Analysis

Representative steady-state PV loops are shown in Figure 1. A summary of the PV loop

analysis is shown in Table 3. Trends to improvement in E_{es}, a rate independent measure of

systolic function, after embolization were seen in the Cilo (Low and High) groups, compared to

Metoprolol and Control animals. No significant change in chamber stiffness (α) or the isovolemic relaxation constant (τ) was seen, demonstrating that diastolic function was not affected by cilobradine or metoprolol therapy in the present study.

Alterations in Calcium-Handling Proteins

Western blots of SERCA2a, NCX1, and RyR2 are shown in Figure 3A. The SERCA2a protein level was significantly reduced and NCX1 markedly increased in the CHF state. These levels of SERCA2a and NCX1 proteins were restored to levels comparable to normal animals in both Meto and Cilo (High) treated animals (Figure 3B).

Although the total RyR2 protein levels were not changed in CHF or after treatment with either metoprolol or cilobradine, PKA phosphorylation of immunoprecipitated RyR2 was significantly increased in chronic failing hearts (Figure 4). Metoprolol and Cilo (High) treatment restored PKA phosphorylation of RyR2 in failing hearts to the levels seen in normal hearts.

Discussion

β-blockade has been shown to prevent the progression of heart failure (Colucci et al.,

1996), improve cardiac performance (Sabbah et al., 1994), and promote reverse remodeling in

failing hearts (Sabbah et al., 1994). Heart rate reduction has been proposed as an important

component of benefit after long-term β-blockade therapy. In the present study, we tested

whether bradycardic therapy can improve CHF and evaluated the effects of a bradycardic agent

with no inotropic actions, cilobradine, on cardiac performance and calcium handling in dogs with

coronary embolization-induced CHF. The primary findings of this study were 1) cilobradine

reduced heart rate at both low and high doses comparable to metoprolol, 2) systolic function was

significantly improved after treatment with cilobradine, and 3) myocardial calcium regulation

was partially restored with cilobradine therapy, similar to metoprolol. These results suggest that

bradycardic therapy without negative inotropic effects, such as seen with cilobradine, may

provide benefit for heart failure patients with systolic dysfunction.

The rationale for heart rate reduction after ischemic injury rests on the intrinsic effect of

lowering the heart rate to improve myocardial oxygen consumption imbalance, as well as long-

term effect on the autonomic control of heart rate.   A greater heart rate reduction and lower

baseline resting heart rates were both associated with improved survival in the Cardiac

Insufficiency Bisoprolol Study II (CIBIS) (CIBIS II Investigators, 1999), similar to findings in

the US Carvedilol Study (Packer et al., 1996). Patients after myocardial infarction also suffer

from autonomic dysregulation of heart rate (Osculati et al., 1990), contributing to higher rates of

mortality and ventricular arrhythmias (ATRAMI Investigators, 1998). As reported by Nagatsu et

al (Nagatsu et al., 2000), dogs treated with β-blockade alone (and subsequently lower heart rates)

were found to have enhanced contractility compared to β-blockade plus pacing (with higher

heart rates). However, both non-pacing and pacing arms received β-blocker treatment, and the

conclusions regarding the sole effect of bradycardia without β-adrenergic blockade on functional

improvement remain limited.

Sinus node inhibitors act to directly inhibit I_f currents (cardiac pacemaker current)

passing through hyperpolarization-activated cyclic nucleotide-gated (HCN) channels, serving to

shift the resting potential closer to the maximal diastolic voltage without altering other phases of

the action potential (Van Bogaert and Pittoors, 2003; Noble, 1984). The most extensively

studied sinus node inhibitor, zatebradine, has been shown to reduce the incidence of ventricular

fibrillation (Hu et al., 2003), reduce infarct size (Hu et al., 2003), and enhance arterial baroreflex

sensitivity, implying higher central and peripheral vagal (autonomic) tone (Kruger et al., 2000).

However, despite lowering early mortality and decreasing infarct size as reported by Hu et al (Hu

et al., 2003) in a rat model, zatebradine induced LV remodeling with concurrent increased

neurohormonal turnover, suggestive of continued sympathetic stimulation. Likewise,

zatebradine produced disappointing results in the treatment of stable angina in patients, failing to

improve time to moderate angina in two separate double-blinded clinical trials (Glasser et al.,

1997; Frishman et al., 1995).

We hypothesized that cilobradine might produce differing results from zatebradine, based

on two key physical properties. Cilobradine produces a use and dose dependent blockade of the

I_f current which is both stronger (82% vs. 36%, respectively) and faster than zatebradine (Van

Bogaert and Pittoors, 2003). As shown elegantly by Van Bogaert et al. (Van Bogaert and

Pittoors, 2003), cilobradine and its racemic mixture also allows unblocking to occur at a much

slower rate than with zatebradine, likely due to a higher association rate for the binding site in

the HCN channel. Early animal studies with cilobradine support our hypothesis. In a study

17

reported by Schmitze-Spanke et al. (Schmitze-Spanke et al., 2004), cilobradine was administered after 60 minutes of coronary occlusion followed by 30 minutes of reperfusion in rabbits; in this model, cilobradine reduced heart rate by 30% and significantly reduced myocardial infarct size.

The present experiment utilizes a sinus node inhibitor, cilobradine, to address if bradycardia as a primary therapeutic endpoint can be used to improve left ventricular function after ischemic injury. In our study, cilobradine effectively reduced heart rate and produced hemodynamic effects similar to metoprolol. Systolic function, as measured by LV dP/dt, was significantly improved after cilobradine, and trends to improvement in EF and end-systolic elastance were evident in all cilobradine treated animals. A significant increase in mean arterial pressure was seen after high dose cilobradine treatment, and increases in LV systolic pressure were evident in all cilobradine treatment groups after CHF, in contrast to control animals. These results compare favorably to the effects of metoprolol on systolic function although to a lesser degree with cilobradine, as shown in previous studies as well as our study, in which increases in MAP and EF were evident after metoprolol (Nagatsu et al., 2000; Sabbah et al., 1994). Most importantly, cilobradine therapy affected ventricular remodeling similar to metoprolol and prevented further increases in ventricular size compared to control animals after CHF. These results are in direct contrast to the effect of chronic zatebradine in rats (Hu et al., 2003), which produced a significant increase in ventricular dimensions after 8 weeks of therapy. Animals treated with metoprolol and high-dose cilobradine, as hypothesized, demonstrated the greatest improvements in ventricular function. As suggested by previous investigators (Lechat, 2003), the correction of myocardial consumption imbalance in heart failure through heart rate reduction and impairment of the sympathetic response with high-dose cilobradine therapy likely led to a sustained decrease in heart size and improved contractility in these animals. Although low-dose

cilobradine produced a significant decrease in resting heart rate, low-dose therapy did not affect

ventricular size or change end-systolic elastance. It is apparent from these results that sinus node

therapy efficacy is dose-dependent, and important cellular actions mediated by I_f, such as heart

rate regulation after stress (Steiber et al., 2006), do not occur at low doses, accounting for crucial

differences in remodeling that are independent of heart rate reduction alone. Finally, the added

benefit of adrenergic blockade with β-blocker therapy must play an important role in inhibiting

neurohormonal activation seen in CHF; although inotropy may be decreased upon initiation,

chronic β-blocker use clearly resulted in the largest improvements after CHF in this study, in

both pressure-volume and echocardiographic indices of systolic function. A wide range of

effects of β-blockade have been documented, including actions on vascular, renal, and

inflammatory pathways. As such, it remains to be seen whether hemodynamic regulation, such

as solely heart rate reduction with sinus node inhibitors, can provide the same degree of reverse

remodeling and, ultimately, long-term mortality reduction as β-blockade. Prospective clinical

trials will be required to address this important issue. Finally, we feel that the degree of heart

failure at the CHF state was equally severe among all treatment groups, based on changes in EF,

LV dP/dt, LVSP, and LVEDP.

The cellular mechanism examined in this experiment is the effect of heart rate reduction

on calcium (Ca^{2+}) handling and function. Abnormalities in cellular Ca^{2+} handling have

consistently been implicated in progressive hemodynamic deterioration (Gwathmey et al., 1987)

and are now considered a fundamental component of heart failure. Precise mechanisms have

focused on the role of Ca^{2+} resequestration into the sarcoplasmic reticulum (SR) by SERCA2a

and Ca^{2+} efflux via NCX1, resulting in low levels of Ca^{+2} release in CHF (Houser et al., 2000).

Although still not completely understood from a functional standpoint, it is clear that increased

NCX1 levels contribute to altered Ca^{2+} homeostasis in CHF, likely in balance with SERCA2a levels, as lowered SERCA2/NCX levels lead to reduced SR Ca^{2+} loading, decreased decay of the Ca^{2+} transient, and resultant negative contractility (Hasenfaus et al., 1999). After induction of CHF through coronary embolization in our study, significant increases in SERCA2a and significant increases in NCX1 were apparent, consistent with previous literature (Gwathmey et al., 1999). After therapy with cilobradine and metoprolol, SERCA2a levels were restored compared to controls, and both metoprolol and cilobradine therapy provided significant reductions in NCX1 levels, suggestive of improved Ca^{2+} handling similar to chronic β-blockade therapy (Gwathmey et al., 1999). Although no changes in protein levels of RyR2 were seen, phosphorylation of the RyR2, which causes defective channel function through dissociation of the regulatory protein FKBP12.6 (Marx et al., 2000), was seen in CHF and was reversed with chronic β-blockade and cilobradine therapy, also consistent with prior literature (Reiken et al., 2003). It is noted that improvement in heart failure after therapy may have accounted for changes in calcium handling proteins rather than the direct actions of bradycardia, which were unable to be determined from the present study. Nevertheless, restoration of Ca^{2+} homeostasis may be an important component of heart rate reduction with cilobradine therapy and may help to partially explain functional improvement.

The limitations of the current experiment must be acknowledged. Although no change was found in prior experiment in sympathetic neurohormones after zatebradine therapy (Hu et al., 2003), serum neurohormonal analysis was not performed in the current study and could corroborate our functional improvements with biochemical data. A complete metabolic analysis, including myocardial enzymes, LDH isoenzymes, and creatinine would also aid in understanding the effect of cilobradine on long-term markers of energy parameters. Measurements of LV mass

were not taken at the time of echocardiography; thus, we are unable to determine the degree, if any, of LV hypertrophy induced. Concurrently, wall stress was not measured.

In conclusion, high-dose cilobradine, a potent sinus node inhibitor that blocks pacemaker I_f currents, effectively reduced heart rate comparable to metoprolol in dogs with coronary-embolization induced CHF. Bradycardia in both cilobradine and metoprolol treated animals was accompanied by significant improvements in left ventricular contractile function, and restoration of calcium handling proteins was evident after both metoprolol and cilobradine treatment. These findings suggest a rationale for bradycardic therapy in the treatment of severe systolic dysfunction and justify further research into clinical application in humans unable to tolerate beta-blocker therapy.

References

ATRAMI (Autonomic Tone and Reflexes After Myocardial Infarction) Investigators, La Rovere MT, Bigger JT, Marcus FI, Mrotara A, Schwartz PJ (1998) Baroreflex sensitivity and heart rate variability in prediction of total cardiac mortality after myocardial infarction. *Lancet* **351**:478-484.

Bristow MR (1984) The adrenergic nervous system in heart failure. *N Eng J Med* **311**:850-851.

CIBIS II Investigators and committees (1999) The Cardiac Insufficiency Bisoprolol Study II (CIBIS II). *Lancet* **353**:9-13.

Colucci WS, Packer M, Bristow MR, Gilbert EM, Cohn JN, Fowler MB, Krueger SK, Hershberger R, Uretsky BF, Bowers JA, Sackner Bernstein JD, Young ST, Holcslaw TL, Lukas MA (1996) Carvedilol inhibits clinical progression in patients with mild symptoms of heart failure. US Carvedilol Heart Failure Study Group. *Circulation* **94**:2800–2806.

Frishman WH, Pepine CJ, Weiss RJ, Baiker WM (1995) Addition of Zatebradine, a Direct Sinus Node Inhibitor, Provides No Greater Exercise Tolerance Benefit in Patients With Angina Taking Extended-Release Nifedipine: Results of a Multicenter, Randomized, Double-Blind, Placebo-Controlled, Parallel-Group Study. *J Am Coll Cardiol* **26**:305-312.

Glasser SP, Michie DD, Thadani U, Baiker WM (1997) Effects of Zatebradine (ULFS 49 CL), a

Sinus Node Inhibitor, on Heart Rate and Exercise Duration in Chronic Stable Angina Pectoris. *Am J Cardiol* **79**:1401-1405.

Gwathmey JKL, Copelas R, MacKinnon R, Shoer FJ, Feldman MD, Grossman W, Morgan JP (1987) Abnormal intracellular calcium handling in myocardium from patients with end-stage heart failure. *Circ Res* **61**:70-76.

Gwathmey JK, Kim CS, Hajjar RJ, Khan F, DiSalvo TG, Matsumori A, Bristow MR (1999) Cellular ad molecular remodeling in a heart failure model treated with the β-blocker carteolol. *AJP-Heart* **45**:H1678-H1690.

Hasenfaus G, Schillinger W, Lehnart SE, Preuss M, Pieske B, Maier LS, Prestle J, Minami K, Just H (1999) Relationship between Na^+-Ca^{2+}-exchanger protein levels and diastolic function of failing human myocardium. *Circulation* **99**:641-648.

He KL, Yi GH, Sherman W, Zhou H, Li Q, Zhang GP, Gu A, Kao R, Haimes H, Harvey J, Roos E, White D, Taylor DA, Wang J, Burkhoff D (2005) Autologous skeletal myoblast transplantation improved hemodynamics and left ventricular function in chronic heart failure dogs. *J Heart Lung Transplant* **24**:1940-1949.

Heilbrunn SM, Shah P, Bristow MR, Valantine HA, Ginsburg R, Fowler MB (1989) Increased β-receptor density and improved hemodynamic response to catecholamine stimulation during long-term metoprolol therapy in heart failure from dilated cardiomyopathy. *Circulation* **79**:483-

490.

Houser SR, Piacentino V III, Weisser J (2000) Abnormalities of calcium cyclings in the

hypertrophied and failing heart. *J Mol Cell Cardiol* **32**:1595-1607.

Hu K, Naumann A, Fraccarollo D, Gaudron P, Kaden JJ, Neubauer S, Ertl G (2003) Heart rate

reduction by zaterbradine reduces infarct size and mortality but promotes remodeling in rats with

experimental myocardial infarction. *AJP-Heart* **286**:1281-1288.

Knecht M, Burkhoff D, Yi GY, Popilskis S, Homma S, Packer M, Wang J (1997) Coronary

endothelial dysfunction precedes heart failure and reduction of coronary reserve in awake dogs.

J Mol Cell Card **29**:217-227.

Kruger C, Landerer V, Zugck C, Ehmke H, Kubler W, Haas M (2000) The bradycardic agent

zatebradine enhances baroreflex sensitivity and heart rate variability in rats early after

myocardial infarction. *Cardiovascular Research* **45**:900-912.

Lechat PP (2003) Beta-Blocker Efficacy According to Heart Rate and Rhythm in Patients with

Heart Failure. Commentary on the Cardiac Insufficiency Bisoprolol Study II Analysis. *Cardiac

Electrophys Rev* **7**:233-235.

Marx SO, Reiken S, Hisamatsu T, Jayaraman T, Burkhoff D, Rosemblit N, Marks AR (2000)

PKA phosphorylation dissociates FKBP12.6 from the calcium release channel (ryanodine

receptor): defective regulation in failing hearts. *Cell* **101**:365-376.

Nagatsu M, Spinale FG, Koide M, Tagawa H, DeFreitas G, Cooper IV G, Carabello BA (2000)
Bradycardia and the Role of β-Blockade in the Amelioration of Left Ventricular Dysfunction.
Circulation **101**:653-659.

Noble D (1984) The surprising heart: a review of recent progress in cardiac electrophysiology. *J Physiol* **353**:1-50.

Osculati G, Grassi G, Giannattasio C, Seravalle G, Valagussa F, Zanchetti A, Mancia G (1990)
Early alterations of the baroreceptor control of heart rate in patients with acute myocardial
infarction. *Circulation* **81**:939-948.

Packer DL, Bardy GH, Worley SJ, Smith MS, Cobb FR, Coleman RE, Gallagher JJ, German LD
(1986) Tachycardia-induced cardiomyopathy: a reversible form of left ventricular dysfunction.
Am J Cardiol **57**:563-570.

Packer M, Bristow MR, Cohn JN, Colucci WS, Fowler MB, Gilbert EM, Shusterman NH (1996)
The effect of carvedilol on morbidity and mortality in patients with chronic heart failure. U.S.
Carvedilol Heart Failure Study Group. *N Engl J Med* **334**:1349–1355.

Reiken S, Gaburjakova M, Gaburjakova J, He KL, Preito A, Becker E, Yi GY, Wang J, Burkhoff
D, Marks AR (2001) β-adrenergic receptor blockers restore cardiac calcium release channel

(ryanodine receptor) structure and function in heart failure. *Circulation* **104**:2843-2848.

Reiken S, Wehrens XH, Vest JA (2003) Beta-blockers restore calcium release channel function and improve cardiac muscle performance in human heart failure. *Circulation* **107**:2459-2466.

Sabbah HN, Shimoyama H, Kono T, Gupta RC, Sharov VG, Scicli G, Levine TB, Goldstein S (1994) Effects of long-term monotherapy with enalapril, metoprolol, and digoxin on the progression of left ventricular dysfunction and dilatation in dogs with reduced ejection fraction. *Circulation* **89**:2852-2859.

Schmitze-Spanke S, Granetzny A, Stoffels B, Pomblum VJ, Gams E, Schipke JD (2004) Effects of a Bradycardic Agent on Postischemic Cardiac Recovery in Rabbits. *J Phys & Pharm* **55**:705-712.

Steiber J, Wieland K, Stockl G, Ludwig A, Hofmann H (2006) Bradycardic and Proarrhythmic Properties of Sinus Node Inhibitors. *Mol Pharm* **69**:1328-1337.

Van Bogaert PP, Pittoors F (2003) Use-dependent blockade of cardiac pacemaker current (If) by cilobradine and zatebradine. *Eur J Pharmacol* **478**:161-171.

Footnotes

*Dr. George and Dr. Cheng contributed equally to this manuscript.

Legends for Figures

Figure 1. Representative Pressure-Volume (PV) Loops at Baseline, Congestive Heart Failure

(CHF), and after 12 weeks of Control (Panel A), treatment with Metoprolol (Panel B),

Cilobradine Low-Dose (Cilo-Low) (Panel C), or Cilobradine High-Dose (Cilo-High) (Panel D).

Figure 2.   Heart Rate (Panel A), LV dP/dt (Panel B), and Ejection Fraction (Panel C) before and

after treatment. (* Meto vs. Control, $p<0.05$) († Meto, Cilo (Low), Cilo (High) vs. Control, all

$p<0.05$) (‡ Control, Meto, Cilo (Low), Cilo (High) vs. Baseline, all $p<0.05$) (§ Meto, Cilo (Low),

Cilo (High) vs. CHF, all $p<0.05$).

Figure 3.   Sarcoplasmic reticulum calcium-ATPase (SERCA2), sarcolemmal sodium-calcium

exchanger (NCX1), and ryanodine receptor (RyR2) protein levels were quantified and

normalized to tubulin at Baseline (Normal), congestive heart failure (CHF), and after Metoprolol

(Meto), and Cilobradine (Cilo) High-dose treatment. Images of Western blot analysis are shown

in Panel A. Panel B shows a significant reduction in SERCA2a after CHF and restoration of

SERCA2a levels after Meto and Cilo. Both Meto and Cilo therapy produced a significant

reduction in NCX1 versus CHF (Panel B) (* $p<0.05$ vs. Normal, † $p<0.05$ vs. CHF). Values

reflect Mean±SD.

Figure 4. Phosphorylation of the ryanodine receptor (RyR2) was measured at normal, in failing

hearts (placebo group, CHF), and after treatment with Metoprolol (Meto) and Cilobradine (Cilo)

High-Dose at 12 weeks. In Panel A, immunoblots probed for both total RyR2 (using 5029 Ab)

and PKA phosphorylated RyR2 with phosphospecific antibody (anti-RyR2-2809P that

recognizes RyR2 PKA phosphorylated on Ser^{2809}). In Panel B, a significant increase in RyR2

phosphorylation (moles of phosphate per mole of RyR2 tetramer) was seen after CHF (*$p<0.05$

vs. Normal), and both Meto and Cilo therapy restored levels to Normal († $p<0.05$ vs. CHF).

Values reflect Mean±SD.

Table 1. Hemodynamics

		Baseline	CHF	12 wks
LVSP (mmHg)				
	Control	127 ± 7	110 ± 3^a	115 ± 5
	Meto	124 ± 2	108 ± 4^a	121 ± 3^b
	Cilo (Low)	130 ± 3	113 ± 3^a	121 ± 4^b
	Cilo (High)	125 ± 3	102 ± 3^a	120 ± 1^b
LVEDP (mmHg)				
	Control	9.5 ± 0.6	22.5 ± 1.4^a	20.2 ± 3.1^a
	Meto	9.2 ± 1.4	20.0 ± 1.4^a	15.2 ± 2.9
	Cilo (Low)	10.2 ± 0.9	22.8 ± 3.4^a	18.8 ± 1.2^a
	Cilo (High)	13.0 ± 2.1	21.0 ± 1.2^a	16.0 ± 3.8
MAP (mmHg)				
	Control	103 ± 5	88 ± 3^a	89 ± 5^a
	Meto	104 ± 3	91 ± 1^a	94 ± 1
	Cilo (Low)	104 ± 2	92 ± 2^a	98 ± 3
	Cilo (High)	100 ± 3	84 ± 2^a	$101 \pm 2^{b,c}$

[a] $p<0.05$ vs. Baseline

[b] $p<0.05$ vs. CHF

[c] $p<0.05$ vs. Control

All data are Mean±SEM

CHF-Congestive Heart Failure, HR-Heart Rate, LVSP-Left Ventricular Systolic Pressure, LVEDP-Left Ventricular End-Diastolic Pressure,

MAP-Mean Arterial Pressure

Table 2. Echocardiography

	Baseline	CHF	12 wks
LVESD (cm)			
Control	2.96 ± 0.20	3.39 ± 0.14[a]	3.56 ± 0.16[a]
Meto	2.73 ± 0.18	3.10 ± 0.17[a]	3.25 ± 0.23[a]
Cilo (Low)	3.15 ± 0.09	3.25 ± 0.14	3.20 ± 0.19
Cilo (High)	3.00 ± 0.21	3.20 ± 0.16[a]	3.20 ± 0.16
LVEDD (cm)			
Control	4.69 ± 0.19	4.75 ± 0.12	4.99 ± 0.14[a,b]
Meto	4.38 ± 0.19	4.54 ± 0.18	4.58 ± 0.13
Cilo (Low)	4.70 ± 0.15	4.64 ± 0.26	4.92 ± 0.34
Cilo (High)	4.61 ± 0.14	4.67 ± 0.19	4.69 ± 0.16

[a] $p<0.05$ vs. Baseline

[b] $p<0.05$ vs. CHF

All data are Mean±SEM

CHF-Congestive Heart Failure, LVESD-Left Ventricular End Systolic Diameter, LVEDD-Left Ventricular End Diastolic Diameter

Table 3. Pressure-Volume Relationships

	Baseline	CHF	12 wks
E_{es} (mmHg/ml)			
Control	7.20 ± 0.99	4.66 ± 0.83^a	$4.06 \pm 1.24^{a,b}$
Meto	8.80 ± 1.26	5.27 ± 1.42	$4.21 \pm 0.92^{a,b}$
Cilo (Low)	5.05 ± 1.45	2.29 ± 0.51	3.42 ± 1.06
Cilo (High)	7.35 ± 1.36	3.56 ± 0.89^a	4.30 ± 0.79
V_0 (ml)			
Control	38.6 ± 5.6	45.2 ± 10.1	48.0 ± 10.0
Meto	37.7 ± 7.8	35.3 ± 10.0	34.0 ± 12.2
Cilo (Low)	36.6 ± 13.7	24.5 ± 18.2	55.1 ± 7.4
Cilo (High)	22.7 ± 4.1	26.2 ± 10.5	29.1 ± 12.8
α			
Control	0.045 ± 0.014	0.040 ± 0.008	0.063 ± 0.020
Meto	0.022 ± 0.004	0.060 ± 0.031	0.029 ± 0.009
Cilo (Low)	0.047 ± 0.021	0.018 ± 0.002	0.016 ± 0.008
Cilo (High)	0.033 ± 0.010	0.047 ± 0.021	0.027 ± 0.006
β			
Control	2.98 ± 2.10	1.54 ± 1.34	0.63 ± 0.46
Meto	4.23 ± 1.14	2.30 ± 1.36	4.17 ± 1.86
Cilo (Low)	2.03 ± 1.66	2.77 ± 0.68	8.06 ± 4.32
Cilo (High)	4.77 ± 3.38	2.56 ± 1.58	5.05 ± 3.83
τ (ms)			
Control	19 ± 5	28 ± 6	40 ± 8
Meto	28 ± 8	34 ± 7	23 ± 7
Cilo (Low)	34 ± 9	48 ± 12	36 ± 9
Cilo (High)	36 ± 5	39 ± 3	37 ± 5

[a] $p<0.05$ vs. Baseline

[b] $p<0.05$ vs. CHF

All data are Mean±SEM

CHF-Congestive Heart Failure, E_{es}-End-Systolic Elastance, V_0-Volume Axis Intercept, α-Chamber stiffness constant, β-scaling constant, E_a-Arterial Elastance, τ-isovolemic relaxation constant, PE-Potential Energy, SW-Stroke Work, PVA-Pressure Volume Area
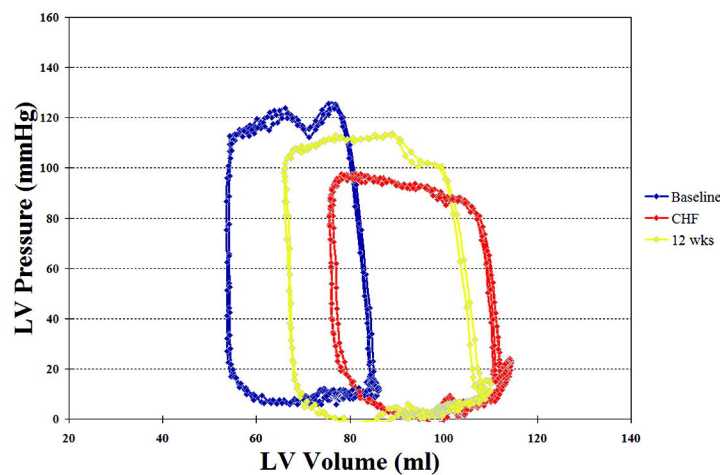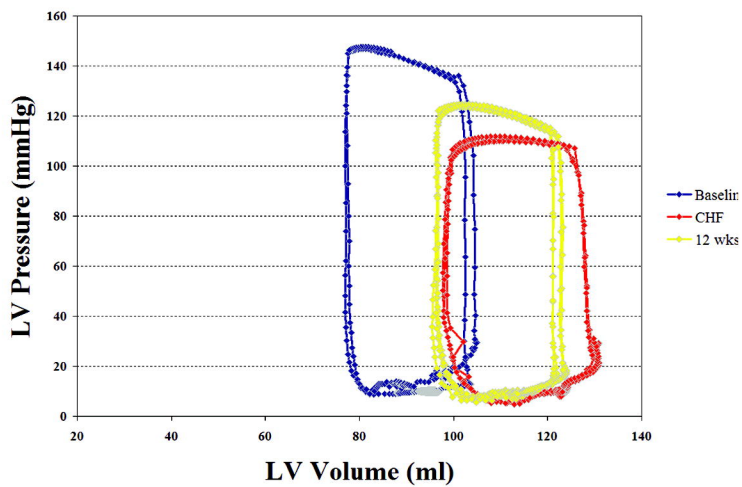
Figure 1

(A)

(B)

(C)

Figure 2

Figure 3

(A)

Normal   CHF   Meto   Cilo

RyR2   ← 560 kD

P2809   ← 560 kD

(B)

Figure 4